

Finite Element analysis of soft boundary effects on the behaviour of shallow foundations

C. Azúa-González, C. Pozo & A. Askarinejad
Department of Civil Engineering and Geosciences, Delft University of Technology, Delft, Netherlands

ABSTRACT: The response of a shallow foundation has been investigated by numerical simulations in a series of $1g$ small scale tests using the Finite Element Method. In this numerical study, special attention has been given to the influence of soft boundaries as a measure to counteract boundary effects, since limitations of space were present in the containers used for the experiments. These experiments were carried out on rigid shallow foundations on sand using strongboxes, which are routinely used in the small beam centrifuge at Delft University of Technology. Two soil constitutive laws were used: 1) the well-known linear elastic perfectly plastic model, and 2) a hypoplastic model. Soft boundaries have been modelled as a continuum, while soil-soft boundary interaction has been addressed by zero thickness interface elements. Model parameters have been back-figured from free field experiments, since boundary effects were considered negligible in these kinds of experiments. Finally, comparisons between numerical and experimental data showed hypoplasticity performed better than the elasto-plastic model to reproduce some aspects of mechanical boundary effects.

1 INTRODUCTION

The response of a shallow foundation is generally evaluated under so-called free field conditions, i.e. other structures or barriers, if present, are far enough to not interfere with the system response. Under these circumstances, classical plasticity solutions are preferred to assess ultimate capacity, whereas physical and numerical modelling techniques are less widely used. However, under constrained conditions the ultimate capacity predicted by analytical expressions as well as the load-displacement (LD) response may be affected. These changes in the foundation response may be properly analyzed using advanced numerical and physical modelling techniques. Among other circumstances, constrained conditions may appear e.g. when small scale tests are performed to evaluate the response of a shallow foundation and space limitations are present in the facilities, as it is the case of the small beam centrifuge at Delft University of Technology (Allersma 1994) or potentially in other geocentrifuges around the world with similar characteristics. Under such limitations, boundary effects should be evaluated with special care, and mitigation strategies should be sought to avoid erroneous conclusions.

Various methodologies have been proposed in the literature to evaluate and potentially minimize hard mechanical boundary effects. These methodologies may be entitled within three broad categories: empirical, numerical, and experimental methods. The reader may refer to Pozo (2016) for a review of these categories. An illustrative example of experimental meth-

ods comes from Pozo et al. (2016), where the influence of hard mechanical boundaries on the response of a shallow foundation was studied through $1g$ small-scale tests. In this experimental study, the influence of boundary effects on LD curves and strain field within the soil was evaluated. The evolution of volumetric and shear strain fields was monitored through Particle Image Velocimetry (PIV) analyses during penetration of the foundation using the MATLAB module GeoPIV-RG (Stanier et al. 2016). These series of experiments were performed in two strongboxes of different size, each one representing a free field and constrained condition, respectively. Through these experiments, Pozo et al. (2016) proved that the implementation of Soft Boundaries (SB) adjacent to strongbox walls was a suitable strategy to reduce mechanical boundary effects under constrained conditions.

In this paper, exemplary tests from Pozo et al. (2016) and Pozo (2016) have been investigated numerically using the Finite Element Method (FEM), aiming to reproduce the influence of SB on the behaviour of a small-scale shallow foundation. Predictions are restricted to $1g$ conditions, since sound experimental evidence has been collected under this situation; however, future research may include similar analyses under Ng conditions. The Finite Element (FE) software package PLAXIS (Brinkgreve et al. 2016) was used for this task. At first, the response under free field conditions is sought to be reproduced, in the sake of back-figuring model parameters. Later, comparisons are carried out between shear

band predictions against experimental evidence collected through PIV analyses. Within this paper, stress and strain variables are presented within Soil Mechanics sign convention.

2 PHYSICAL MODELLING

2.1 Soil characteristics

Merwede River sand was used in this series of tests. It is a uniform silica sand which consists of sub-angular to sub-rounded particles with a mean particle size d_{50} of 0.92 mm and a specific gravity G_s of 2.65 (Poza 2016). The sand has a mean uniformity coefficient of 1.3; whereas the minimum and maximum void ratio have been reported to be $e_{min} = 0.52$ and $e_{max} = 0.72$. Later, soil packing state will be referred by its relative density $RD = 100 \cdot (e_{max} - e_0) / (e_{max} - e_{min}) [\%]$, where e_0 is the initial void ratio.

2.2 Experimental setup

The experimental database produced by Poza (2016) corresponds to tests developed in dry sand. Samples were prepared through the travelling pluviation method (Lo Presti et al. 1992) aiming to reproduce specimens with uniform relative densities within 55 to 93 %. Two strongboxes were used, which were made up of aluminium, PVC and transparent acrylic glass. Hereafter, these strongboxes will be referred as FB (free field condition) and CB (constrained condition). A steel strip footing with dimensions 30 mm x 50 mm (height x width) was used. This footing covered the full strongbox breadth, aiming to ensure plain strain conditions perpendicular to the front acrylic glass. A sketch of the experimental setup is shown in figure 1.

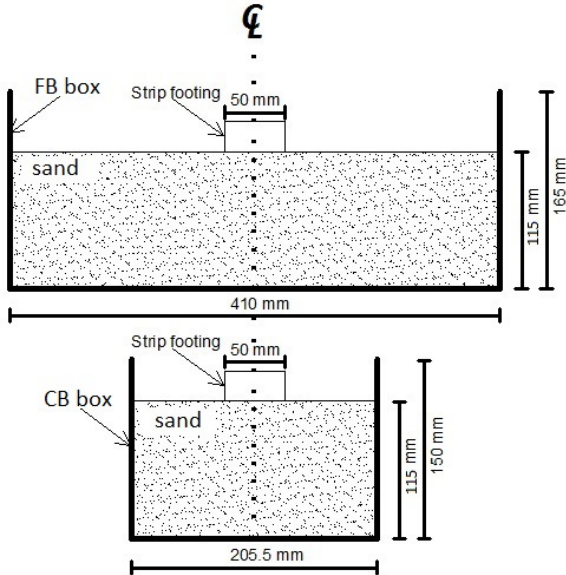


Figure 1: Sketch of free field (SB-F) and constrained (SB-S) strongboxes used for plain strain penetration tests.

2.3 Boundary conditions (BC)

Two types of lateral BC were implemented in the experimental setup:

1. BC1: A hard boundary of aluminium or PVC was used. For the sake of simplicity, both materials were assumed to provide a large rigidity relative to the stiffness of the soil.

2. BC2: A layer of rubber material (shore hardness of 8 – 13A) was added between the sand and the hard lateral boundary to simulate a SB, where rubber padding thickness was set to 9mm.

Independently of the lateral BC type, a sandpaper of a grit size of P150 (100 μ m of average particle size) has been located between the soil and the soft or hard boundary. This procedure was aimed to enable a uniform roughness between the soil and lateral container boundaries. The FB-container was used only with a lateral boundary of the BC1 type, since a free field condition was ensured due to the large longitudinal dimension of the strongbox ($\text{length}_{\text{strongbox}} / \text{width}_{\text{footing}} = 8.2$). These type of tests will be referred as case 1. In addition, experiments performed within the CB-container combined with BC1 and BC2 lateral conditions will be referred as case 2 and case 3, respectively. The first combination aimed to mimic a constrained condition; whereas the latter sought to explore SB effects under constrained conditions. A summary of strongbox type and BC used for the three cases is shown in table 1.

Table 1: Strongbox type and BC for different cases.

Case	Strongbox type	lateral BC
1	FB	BC1
2	CB	BC1
3	CB	BC2

2.4 Load-displacement data and image acquisition

Load-displacement data has been collected during footing penetration under displacement-controlled conditions (constant rate of 0.08 mm/s). In addition, this force-displacement data has been complemented through an image acquisition process (rate of 2 images/second) for further PIV analyses (Poza 2016). The image acquisition process was carried out using a digital-single lens reflex camera (Canon EOS 750D) aided with continuous illumination through a lamp (~ 800 lumens of luminous flux) positioned 500 mm away from the strongbox; while the camera was located 300 mm away. An illustration of the data acquisition process is shown in figure 2.

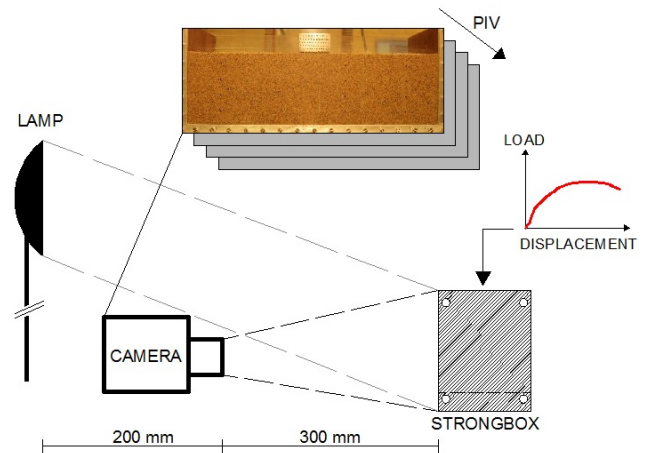


Figure 2: Sketch of parallel acquisition of illumination-aided images and load data during displacement-controlled tests.

2.5 LD curves from experimental results

Hard mechanical boundary effects were reflected in three features of the LD data in terms of pre-peak response, i.e. an increased bearing capacity and initial stiffness, and occurrence of peak state at a shorter penetration depth. While in terms of post-peak response, a sharper reduction of load and a lower residual bearing capacity was observed under constrained conditions. The three pre-peak aspects could be satisfactorily modified by the implementation of rubber paddings (case 3), i.e. the stiffness and bearing capacity was decreased, and peak state occurred at a larger penetration depth when compared to case 2. Nevertheless, post-peak response could not be modified significantly, as observed in figure 3.

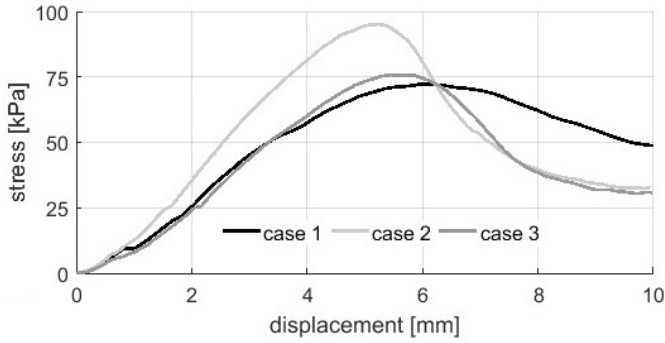


Figure 3: LD curves from experimental results.

3 NUMERICAL MODELLING

Plain strain FE models were used in all cases. Model domain was restricted laterally to half of the corresponding strongbox size due to the ideally symmetric configuration of the experiments, while full soil specimen depth ($H_{soil} = 115$ mm) was considered in the vertical axis. Soil and soft boundaries were modelled by means of 15-noded triangular elements. Regardless of the boundary type (BC1 or BC2), soil elements and virtual hard or soft boundaries were connected by means of 10-noded interface elements to mimic the influence of sandpaper on soil-SB interaction. Domain boundary conditions for case 1 and case 2 were set as normally fixed and fully fixed in the lateral and bottom boundaries, respectively. However, the bottom boundary was set as normally fixed in case 3, to allow horizontal movement at the base of the SB to be consistent with experimental observations through image analyses. For the sake of simplicity, the steel footing has been considered as fully rigid since a large bending stiffness compared to soil stiffness is expected under $1g$ conditions. Therefore, footing penetration has been modelled using uniform prescribed displacements at the top of the specimen level as shown in figure 4.

3.1 Constitutive laws

3.1.1 Soil

Two constitutive models were chosen, namely 1) a linear elastic perfectly plastic (LEPP) model within a Mohr-Coulomb failure criterion and non-associative

plasticity (Vermeer 1982), which has been adopted with a tension cut-off at the planes $\sigma'_1 = \sigma'_2 = \sigma'_3 = 0$ in the principal stress space since a small cohesion $c' = 0.1$ kPa has been imposed to prevent premature soil collapse at the top level; and 2) the hypoplasticity model from von Wolffersdorff (1996).

Unlike most elasto-plastic constitutive laws, the hypoplastic model treats the void ratio e , and the Cauchy stress tensor σ' as state variables. This enables the model to capture the mechanical response at different packing and stress states within a unique parameter set. As other hypoplastic relations¹, this constitutive law is rate-independent and incrementally non-linear in the current strain rate $\dot{\epsilon}$; and can be expressed by a single tensorial formulation as depicted in equation 1:

$$\dot{\sigma}'(\sigma', e, \dot{\epsilon}) = \mathfrak{L}(\sigma', e) : \dot{\epsilon} + \mathbf{N}(\sigma', e) \|\dot{\epsilon}\| \quad (1)$$

where $\dot{\sigma}'$ is the (objective) Jaumann stress rate tensor, $\mathfrak{L} = f_b f_e (F^2 \mathfrak{S} + a^2 \hat{\sigma}' \otimes \hat{\sigma}') / (\hat{\sigma}' : \hat{\sigma}')$ is a fourth order tensor with \mathfrak{S} being the fourth order unit tensor, and $\mathbf{N} = f_d f_b f_e F a (\hat{\sigma}' + \hat{\sigma}'_d) / (\hat{\sigma}' : \hat{\sigma}')$ is a second order tensor. Both tensors are a function of the normalized stress tensor $\hat{\sigma}' = \sigma' / \text{tr}(\sigma')$, while \mathbf{N} is also dependent on the deviatoric part of the normalized stress tensor $\hat{\sigma}'_d = \hat{\sigma}' - (1/3)\mathbf{I}$ with \mathbf{I} being the second order unit tensor. Critical states are incorporated in the formulation by the scalar-valued function $F = f(\hat{\sigma}'_d)$ and the parameter $a = \sqrt{3/8}(3/\sin(\phi'_{cv}) - 1)$. The scalar factors f_e, f_d cope with the influence of density; whereas f_b reflects the effect of stress level. Due to space limitations, the reader may refer to Herle and Gudehus (1999) for further details on parameter calibration.

3.1.2 Soft boundary (SB)

Rubber paddings have been modelled through isotropic linear elasticity, defined by two parameters, namely the Young's modulus $E_{sb} = 0.271$ MPa as measured from unconfined compression tests (Pozo 2016), and Poisson's ratio ν_{sb} for rubber, which was adopted as 0.49 to address its widespread volumetric incompressibility.

3.2 Soil - boundary interaction

Interaction between soil and (rigid or soft) domain boundaries has been addressed using zero-thickness interface elements, which may represent a zone of soil with degraded stiffness and strength properties. This interface elements connect couples of nodes, enabling gapping or slipping to occur. The elastic relative displacements which may occur in these interfaces are governed by the interface elastic constants K_N and K_S ; where $K_N = E_{oed,i}/t_v$ and $K_S = G_i/t_v$ are the interface elastic constants with t_v being the interface virtual thickness. Interface oedometric stiffness $E_{oed,i}$ and shear modulus G_i are computed from elastic properties of the adjacent soil including a degradation factor R and a Poisson's ratio $\nu_i = 0.45$, i.e.

¹The term hypoplasticity may reference to three different theories, namely Karlsruhe-hypoplasticity, Dafalias-hypoplasticity and CLoE-hypoplasticity. The first meaning is adopted here

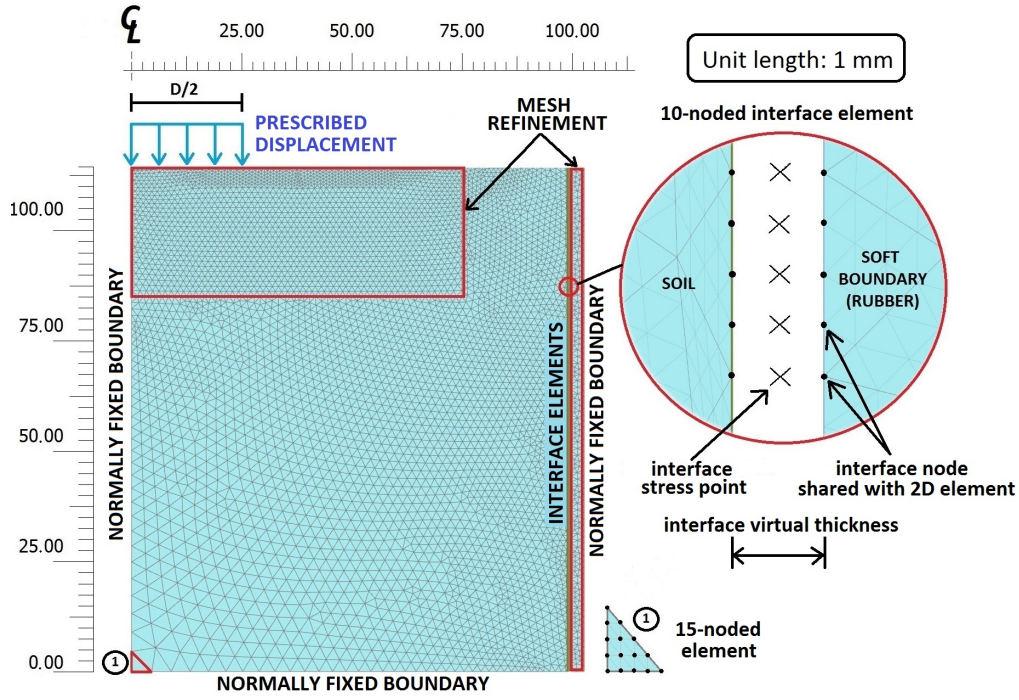


Figure 4: Elucidation of a typical (very fine) mesh for simulations corresponding to case 3 tests: 10207 elements, 82704 nodes

$G_i = R^2 G_{soil}$ and $E_{oed,i} = 2G_i(1 - \nu_i)/(1 - 2\nu_i)$. In the sake of simplicity, the virtual thickness t_v has been set to 10% of the average element size.

In these interface elements, non-associative plasticity governs the flow rule within a yield surface of the Mohr-Coulomb type with a nil dilatancy angle ψ'_i . Strength reduction is achieved in a similar manner as carried out for the interface stiffness. In this case, the relations $\tan(\phi'_i) = \tan(\phi')/R$ and $c'_i = c'/R$ have been adopted. It is worth to mention that when soil behaviour has been set to be hypoplastic, the interface yield locus has been removed to avoid convergence problems (by deactivating interface elements). Furthermore, when this advanced constitutive law has been used, a reference interface shear modulus has been estimated as $G_i^{ref} = R^2 E_{50}^{ref}/[2(1 + \nu')]$, with $\nu' = 0.3$ and $E_{50}^{ref} = 600RD[KPa]$ for a reference pressure of $100kPa$ (Brinkgreve et al. 2010). In addition, a rate of stress dependency $m = 0.5$ (typical value for sands) has been adopted. The reduction factor R has been adopted as 0.75 independently of the soil constitutive law, in the sake of simulating a rough soil - boundary interface (as intended with the implementation of sandpaper in the experimental setup).

3.3 Finite Element mesh

Three kinds of mesh density have been applied as available by default in PLAXIS, i.e. medium, fine and very fine mesh. The difference lies on the average element size l_{avg} , which can be computed as $l_{avg} = 0.06r_e \sqrt{x_{max}^2 + y_{max}^2}$, where r_e takes the default values of 1.00, 0.67 and 0.50 for medium, fine and very fine mesh configurations, respectively; and x_{max} and y_{max} are the maximum horizontal and vertical lengths of the model domain, respectively. In addition, strategic mesh refinement zones have been

adopted in the vicinity of the footing corner to improve the quality of displacement and strain fields, and within soft boundaries as shown in figure 4.

3.4 Stress field initialization

Soil initial stress field under $1g$ conditions has been generated using the so-called k_0 - procedure. In this procedure, only soil clusters are present and gravity loads are applied. These loads derive from the (dry) soil unit weight γ_{soil} . Required values of γ_{soil} have been estimated as a function of the initial void ratio, i.e. $\gamma_{soil} = \gamma_{water} G_s / (1 + e_0)$. Effective vertical stresses σ'_{yy} are calculated to comply with equilibrium in terms of body forces. Nevertheless, the effective lateral stress is back-figured from σ'_{yy} based on the coefficient of earth pressure at rest k_0 , i.e. $\sigma'_{xx} = k_0 \sigma'_{yy}$. Required k_0 -values have been estimated empirically as suggested by Jacky (1944), i.e. $k_0 \approx 1 - \sin \phi'$, where ϕ' is the friction angle. Values of this parameter have been obtained using the empirical formula for sands $\phi' \approx 28 + 12.5RD/100$ [°] (only for stress initialization), derived by Brinkgreve et al. (2010) using regression analysis on experimental data from Jefferies and Been (2006). This procedure enabled to obtain a realistic initial stress field, regardless of the chosen constitutive law. Soft boundaries, if present, were simulated using $\gamma_{rubber} = 11.0 \text{ KN/m}^3$ as wished-in-place, by switching soil material models into soft boundary material. This initialization process caused inevitably artificial soil displacements, which were reset before further calculations were carried out.

3.5 Displacement-controlled tests

Footing displacement-controlled tests were modelled through sequential calculation phases involving small prescribed displacement increments, i.e. 1 mm per calculation phase. Within each calculation phase,

the maximum prescribed displacement increment has been set to 1% per step to ensure that at least 100 steps are computed within each 1 mm of footing displacement. This procedure aided to reduce the required number of iterations per step. Soil collapse in the FEM simulations has been considered to be reached if the automatic load-increment routine is unable to proceed with increasing prescribed displacements (after trial-and-error a reasonable upper bound of maximum number of iterations per step was found to be ~ 60). Finally, Load-displacement curves have been elaborated by post-processing the vertical reaction force (per width) at model boundaries (induced by prescribed displacement increments only).

4 NUMERICAL RESULTS AND DISCUSSION

4.1 Back-analysis of model parameters

Tests corresponding to case 1 were chosen for inverse analysis, primarily because of the nearly negligible interaction of the strongbox boundaries with the adjacent soil. Model parameters were adjusted wisely by trial-and-error until a reasonably good agreement was achieved between experimental and numerical data.

In general, each parameter tend to dominat different features of the mechanical response. For instance, when the linear elastic perfectly plastic model was used, the Young's modulus controlled the slope of LD curves. Therefore, this parameter was changed upon an initial good agreement in terms of the secant slope of LD data, while the Poisson's ratio was set to 0.3 (typical value for soils). As an initial guess of strength parameters, the approximation $\phi' - \psi \approx 30^\circ$ (Brinkgreve et al. 2010) was adopted, while keeping a reasonable value of ϕ' . In general, final tuning between numerical and experimental data required refinement of all the parameters, since they interact between each other to some extent.

Similarly, when hypoplasticity was used, some parameters were fixed according to correlations from Herle and Gudehus (1999) and recommendations by Bauer (1996). Correlations for characteristic void ratios in terms of minimum and maximum void ratios were adopted, namely $e_{i0} = 1.2e_{max}$; $e_{c0} = e_{max}$; $e_{d0} = e_{min}$. The exponent β was set to 1.0, which may be valid for a wide range of sands. In addition, typical ranges were used to narrow possibilities during parameter adjustment, i.e. $0.10 < \alpha < 0.30$ and $0.18 < n < 0.40$.

The non-linearity of stiffness in LD curves could not be captured when the LEPP model was used, as observed in Figure 5. This can be explained by the fixed Young's modulus of the constitutive law (no stress dependency of stiffness is taken into account), and its incapacity to take into account the void ratio dependency of stiffness in the soil. Nevertheless, the average trend of LD response could be captured within a proper choice of Young's Modulus. Therefore, parameter selection was focused to force fitting

in terms of peak state only. This drawback was observed to be less severe under looser samples, where non-linearity is less pronounced during pre-peak response. In addition, it is clarified that only pre-peak response was studied with the LEPP model since no softening behaviour is included in the formulation.

On the other hand, the pre- and post-peak evolution of stiffness was intended to be captured when a hypoplastic model was used. Remarkably, strain softening-like behaviour was poorly captured by the hypoplastic model; unveiled by sudden load drops as shown in figure 6. In this case, it was difficult to match both pre- and post-peak behaviour for all relative densities within a unique parameter set. The chosen parameter set performed better for a dense packing state ($RD = 92 - 93\%$) at the expense of a poor post-peak response for a looser state ($RD = 59\%$). Parameters were chosen on purpose to perform better at a dense state because further numerical investigations are focused in dense samples only, where boundary effects may be more pronounced (Pozo et al. 2016). Tables 2 and 3 summarize back-figured model parameters and interface parameters, respectively.

Table 2: Soil constitutive model parameters

LEPP model							
RD [%]	E [kPa]	ν'	c' [kPa]	ϕ' [°]	ψ' [°]		
93	800	0.3	0.1	48.00	25.00		
75	650	0.3	0.1	45.00	21.50		
59	470	0.3	0.1	42.70	18.60		
Hypoplasticity							
ϕ'_{cv} [°]	h_s [MPa]	n	α	β	e_{i0}	e_{c0}	e_{d0}
37.0	920	0.18	0.15	1.0	0.86	0.72	0.52

Table 3: Soil - (hard or soft) boundary interface parameters

LEPP model					
RD [%]	G_i [kPa]	$E_{oed,i}$ [kPa]	c'_i [kPa]	ϕ'_i [°]	ψ'_i [°]
93	173	1904	0.075	39.80	0.0
75	141	1547	0.075	36.90	0.0
59	102	1119	0.075	34.70	0.0
Hypoplasticity					
RD [%]	G_i^{ref} [kPa]	$E_{oed,i}^{ref}$ [kPa]	p_{ref} [kPa]	m	
93	12072	132793	100	0.5	
59	7659	84245	100	0.5	

The influence of mesh density was negligible when the linear elastic perfectly plastic model was used; nevertheless, mesh density was observed to have major effect with hypoplasticity, as observed in figure 7. Therefore, back-figured model parameters were chosen to ensure fitting when a very fine mesh configuration was used.

4.2 Validation against Direct Shear (DS) tests

Hypoplastic model parameters have been validated against experimental data on DS tests. These tests were carried out on (dry) medium dense sand samples ($RD = 75\%$) under 16 kPa, 60 kPa and 103 kPa of normal load. A plot for comparison between numerical simulations and experimental data is shown in

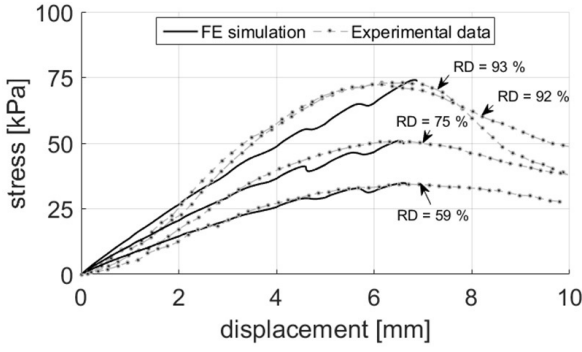


Figure 5: LD curves for case 1: LEPP model (very fine mesh).

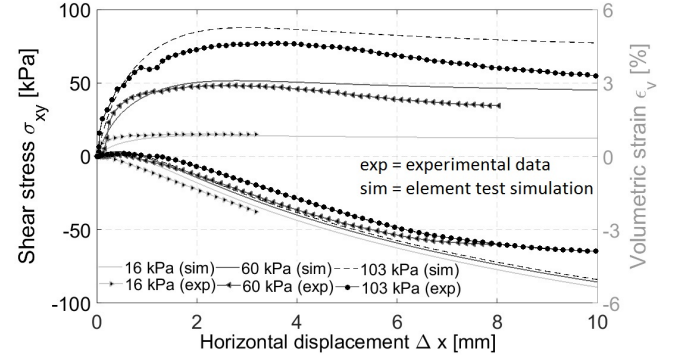


Figure 8: Shear stress and volumetric strain response on DS tests.

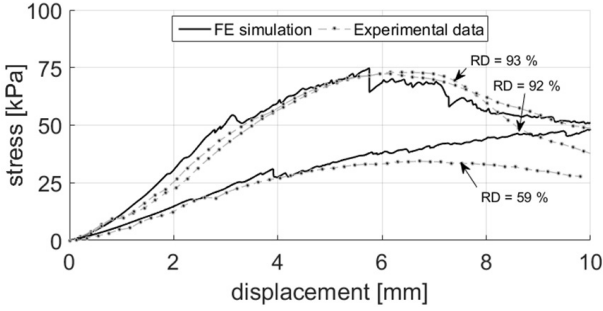


Figure 6: LD curves for case 1: hypoplasticity (very fine mesh).

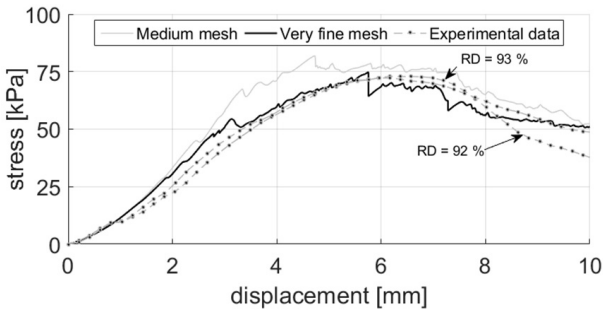


Figure 7: Mesh sensitivity for case 1 using hypoplasticity.

figure 8. Numerical simulations were observed to approximate better the experimental results for tests under low normal loads; whereas for medium loads, the hypoplastic model showed underprediction of shear stress and an overprediction of dilatancy. Differences between predictions and experimental data has been quantified by the Root Mean Square Error (RMSE), which has been normalized by the residual shear stress and volumetric strain after 10 mm of horizontal displacement. The normalized RMSEs in terms of shear stresses have been found to be 15.9%, 20.1% and 25.2% for samples under 16 kPa, 60 kPa and 103 kPa of normal load, respectively; whereas in terms of volumetric strains, RMSEs were determined to be 10.4%, 8.5% and 15.2% for samples under 16 kPa, 60 kPa and 103 kPa of normal load, respectively. These element test validations showed that the back-figured model parameters possessed better predictive capabilities in terms of volumetric strains than for shear stresses.

4.3 Comparisons with PIV for cases 2 and 3

Numerical predictions for a dense sand ($RD = 93\%$) in terms of shear strains are presented in figure 9 (a) & (b) and (c) & (d) for cases 1 and 2, respectively. Figures 9 (a) and (b) show that shear band develop-

ment for case 1 could be captured reasonably well by both constitutive laws. In both cases, shear band (horizontal) extension was in agreement with PIV results; however, shear band depth and inclination with respect to the horizontal plane near shear band tail were underestimated, whereas shear band inclination beneath the footing was overpredicted.

As discussed in the literature, shear band inclination θ with respect to the major principal stress direction may show dependency on the friction angle (Mohr-Coulomb theory: $\theta = \pi/4 - \phi'/2$) and on the dilatancy angle (Roscoe (1970): $\theta = \pi/4 - \psi'/2$; Arthur et al. (1977): $\theta \approx \pi/4 - \phi'/4 - \psi'/4$). For both constitutive laws, the major principal stress direction showed the tendency to be rotated from a nearly vertical direction within the soil beneath the footing into a nearly horizontal direction within the soil near shear band tail. Therefore, this tendency of major principal stress direction rotation combined with too high values of friction angles (ϕ' and ϕ'_{cv}) and the overprediction of dilatancy (too high values of ψ' in LEPP parameters and overprediction of dilatancy as discussed in section 4.2) may have been the cause of an inadequate prediction of shear band inclination (underprediction of θ) within both constitutive laws. In addition, this poor predictive capability of both constitutive models in terms of shear band inclination may be a major contribution to the underprediction of shear band depth for both constitutive laws, since it affects shear band geometry.

In case 2, shear band depth was observed to be reduced through image analyses (see figure 9). Remarkably, only the hypoplastic model showed qualitatively this behaviour when compared to the prediction for case 1. On the other hand, a deeper shear band branch was predicted to be developed by the LEPP model. This resulted in reflected shear bands adjacent to the lateral boundary within an inclination of $45^\circ - \phi'/2$ ($\phi' = 48^\circ$), which may have erroneously suggested the occurrence of passive thrust.

4.4 Effect of mechanical boundaries on LD curves

4.4.1 FEM simulation of case 2

In this case, the LEPP model was not able to capture neither an increase in stiffness response and bearing capacity properly, nor a reduction in Peak State Penetration Depth (PSPD). Based on the experimental re-

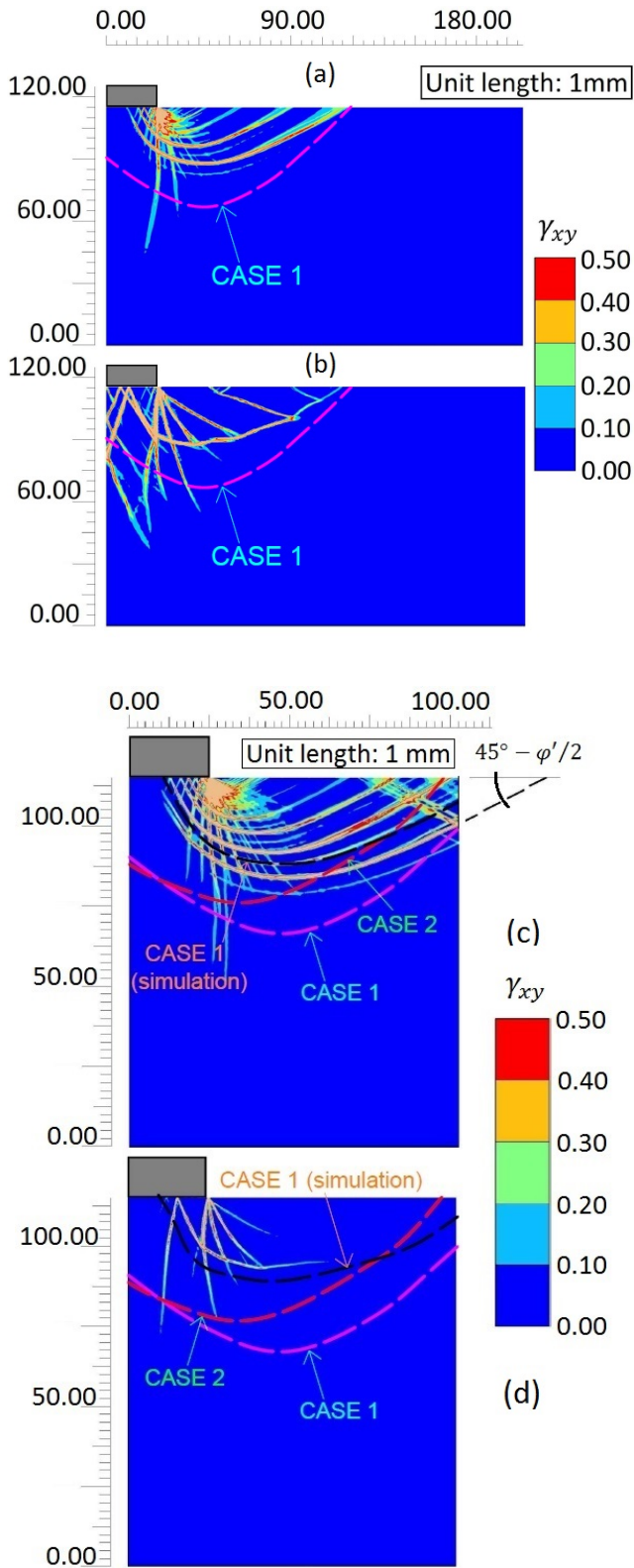


Figure 9: Shear strain field for cases 2 and 3 ($RD = 93\%$): a) & c) LEPP model and b) & d) hypoplasticity. Shear band from experiments and case 1 simulations are shown with dashed lines.

sults, the peak secant stiffness was expected to be increased in 51.1%; the bearing capacity in 31.2%; and the PSPD to be reduced in 13.4%. However, the LEPP model predicted only 2.6% of increase in peak secant stiffness; an increase of 1.1% in bearing capacity; and a reduction of 1.4% in PSPD, i.e. hard mechanical boundary effects on the LD response were erroneously predicted to be negligible under a constrained condition. On the other hand, the hypoplastic model performed better in predicting an increased bearing

capacity within 5.0% of error with respect to the experimental observation; however, it overpredicted the secant stiffness response by 35.8% and underpredicted the PSPD by 22.7%. In addition, no post-peak response could be captured since soil (numerical) collapse was obtained after the peak state occurred. Remarkably, the initial stiffness response until 2 mm of penetration was in good agreement with the experimental result when hypoplasticity was used; whereas a good agreement was observed only until 1 mm of penetration for the LEPP model. The poor predictive performance of the LEPP model in terms of key aspects of hard mechanical boundary effects could be attributed to the lack of stiffness stress dependency in its formulation. On the contrary, the better performance of hypoplasticity in capturing the influence of hard mechanical boundaries on the bearing capacity may be explained after the anisotropy and barotropy dependence of stiffness. Nonetheless, it should be noticed that poor capturing of strain-softening of the hypoplastic model was reflected again in sudden sharp load drops during strain localization. Finally, the premature (numerical) soil failure predicted at a penetration depth of 4.1 mm might be explained after this drawback of the model. Predictions of case 2 for a dense sand ($RD = 93\%$) are shown in figure 10.

4.4.2 FEM simulation of case 3

When case 3 was simulated using a LEPP model, the peak secant stiffness remained nearly unchanged within a reduction of 3.3% (percentage taken with respect to its numerical prediction of case 1). This supports the previous discussion on the insensitivity of the model to properly capture changes on LD stiffness as a boundary effect, due to the lack of pressure and void ratio dependency of stiffness in its formulation. Moreover, it erroneously predicted an increase of bearing capacity with respect to its numerical prediction for case 2 within 8.0%; contradictory to the expected reduction of bearing capacity when SB are implemented under constrained conditions (based on the experimental observations in section 2.5). This analysis revealed a poor predictive capacity of the LEPP model in terms of capturing hard and soft boundary effects.

On the other hand when case 3 was simulated using hypoplasticity, a reasonably good agreement in terms of bearing capacity was obtained. In this situation, the bearing capacity was predicted to be reduced with respect to its numerical prediction for case 2; consistent with experimental observations. This predicted bearing capacity was only 3.3% below the one measured experimentally in case 3. Nonetheless, the hypoplastic model overpredicted the initial stiffness, which resulted in an underprediction of the PSPD of 43.6% with respect to the experimental result. In this situation, a reduction of peak secant stiffness was captured as expected from experimental evidence; however, yet this reduction was quantified in 10.3% only, against a reduction of 28.9% as measured experimen-

tally. Regarding post-peak response, the hypoplastic model overpredicted the residual load at 10 mm of footing penetration by a factor 25.2% with respect to the experimental result. This revealed hypoplasticity was able to predict most of the aspects of hard and soft boundary effects qualitatively. Moreover, it proved to have a good predictive capability of the influence of mechanical boundary effects in terms of bearing capacity. Nevertheless, a poor capacity to mimic strain-softening like behaviour was witnessed in case 3 as well, observed as sudden load drops which were persistent during post-peak response. In addition, the poor capacity of the model to capture properly the initial stiffness may be attributed to calibration-related problems. For instance, the parameter β which influences the size of the response envelop (therefore it affects the bulk and shear stiffness) has been adopted as 1.0 (typical for sands) during back-analysis because no further lab experiments were available at the moment numerical predictions were made. However, this dimensionless parameter controls the response under proportional stress paths such as oedometric compression (Herle and Gudehus 1999). Therefore, potential inaccuracies in the calibration of the β parameter may have influenced on the response of case 2 and 3, since these constrained conditions may be fairly considered to approach an oedometric condition. This suggests potential issues related to the uniqueness of the solution; however, such a discussion may exceed the scope of the current study.

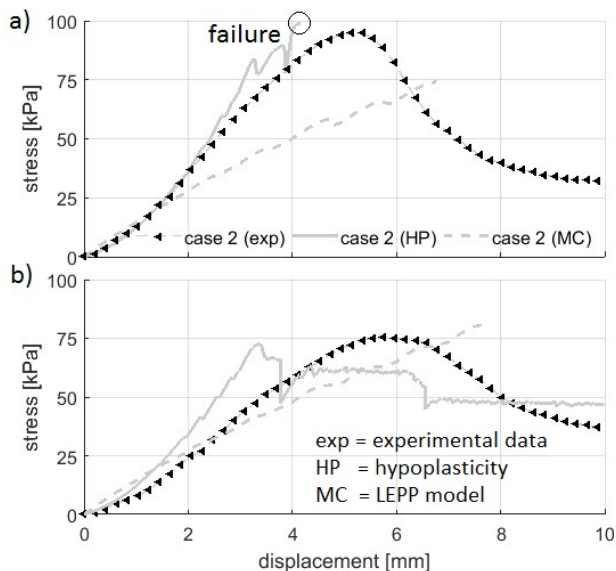


Figure 10: LD curves ($RD = 93\%$): a) case 2, b) case 3.

5 CONCLUSIONS

A numerical investigation of the behaviour of a shallow foundation has been carried out using FEM, providing special attention to boundary effects. A LEPP and a hypoplastic model were used. Through this investigation, drawbacks of both constitutive laws have been revealed. The first constitutive law was unable to capture typical mechanical boundary effects, even after it proved to work reasonably well for free field

conditions. Only the second law was able to reproduce some typical boundary effects, i.e. under constrained conditions, an increased ultimate capacity and larger stiffness was predicted, consistent with experimental evidence; however, premature soil failure prohibited to capture post-peak response (potentially attributed to the poor capacity of hypoplasticity to capture strain-softening like behaviour). When SB were modelled, a drop in ultimate capacity was observed, which was in agreement with experiments; nevertheless, the initial stiffness was overpredicted. As a result, the capacity of hypoplasticity to capture most of the aspects of hard and soft mechanical boundary effects has been shown.

Acknowledgements. Financial support provided to the first two authors by SENESCYT (Ecuador) is gratefully acknowledged. The authors would like to thank the assistance provided by Wim Verwaal and Arno Mulder during lab testing.

REFERENCES

- Allersma, H. (1994). The University of Delft Geotechnical Centrifuge. In *Proceedings of the International Conference Centrifuge 94*, pp. 47–52.
- Arthur, J. F. R., T. Dunstan, Q. A. J. Assadi, & A. Assadi (1977). Plastic deformation and failure in granular materials. *Géotechnique* 27, 53–74.
- Bauer, E. (1996). Calibration of a comprehensive hypoplastic model for granular materials. *Soils and Foundations. Japanese Geotechnical Society* 36(1), 13–26.
- Brinkgreve, R. B. J., E. Engin, & H. K. Engin (2010). Validation of empirical formulas to derive model parameters for sands. In *Numerical Methods in Geotechnical Engineering*, pp. 137–142.
- Brinkgreve, R. B. J., S. Kumarswamy, & W. Swolfs (2016). *PLAXIS Manual*. Delft, Netherlands.
- Herle, I. & G. Gudehus (1999). Determination of parameters of a hypoplastic constitutive model from properties of grain assemblies. *Mech. Cohes.-Frict. Mater.* 4, 461–486.
- Jacky, J. (1944). The coefficient of earth pressure at rest. *Journal of Hungarian Architects and Engineers*, 355–358.
- Jefferies, M. & K. Been (2006). *Soil Liquefaction: A critical state approach*. Abingdon, UK: Taylor & Francis.
- Lo Presti, D. C., P. Sergio, & C. Virginio (1992). Maximum dry density of cohesionless soils by pluviation and by ASTM D 4353-83. A comparative study. *Geotechnical Testing Journal* 15, 180–189.
- Pozo, C. (2016). Soft Boundary Effects (SBE) on the behaviour of a shallow foundation. Master's thesis, Delft University of Technology, Delft, Netherlands.
- Pozo, C., Z. Gng, & A. Askarinejad (2016). Evaluation of Soft Boundary Effects (SBE) on the behaviour of a shallow foundation. In *3rd European Conference on Physical Modelling in Geotechnics*, Nantes, France, pp. 385–390.
- Roscoe, K. H. (1970). The influence of strain in soil mechanics. *Géotechnique* 20, 129–170.
- Stanier, S. A., J. Blaber, W. A. Take, & D. White (2016). Improved image-based deformation measurement for geotechnical applications. *Canadian Geotechnical Journal* 53(5), 727–739.
- Vermeer, P. A. (1982). A five-constant model unifying well-established concepts. In *International Workshop on Constitutive relations for Soils*, Grenoble, pp. 175–198.
- von Wolffersdorff, P. A. (1996). A hypoplastic relation for granular materials with a predefined limit state surface. *Mech. cohesive - frictional mater.* 1, 251–271.